ISSN 1029-9599, Physical Mesomechanics, 2021, Vol. 24, No. 1, pp. 77–84. © Pleiades Publishing, Ltd., 2021.
Russian Text © The Author(s), 2020, published in Fizicheskaya Mezomekhanika, 2020, Vol. 23, No. 3, pp. 43–53.

Very High Cycle Fatigue of D16T Aluminum Alloy

A. A. Shanyavskiy[1,2]*, A. D. Nikitin[2], and T. Palin-Luc[3]

[1] *Aviation Register of the Russian Federation, Sheremetyevo Airport, Moscow region, 141426 Russia*
[2] *Institute of Computer Aided Design, Russian Academy of Sciences, Moscow, 123056 Russia*
[3] *Arts et Metiers Institute of Technology, CNRS, University of Bordeaux, Bordeaux, 33405 France*
** e-mail: 106otdel@mail.ru*

Received May 18, 2020, revised May 18, 2020, accepted May 25, 2020

Abstract—The paper provides a fractographic analysis of fatigue cracking in D16T aluminum alloy under very high cycle fatigue at a frequency of 20 kHz. The analysis shows that in the range of 2.8×10^8 to 5.1×10^9 cycles to failure, the material reveals cracks on and beneath its surface with their subsurface site developing through intergranular fracture at triple junctions or smoothly faceted transgranular fracture. The main crack develops by shear with the formation of differently oriented facets against which a cascade of oriented and misoriented dimples appears. Such dimples are left by spherical and ellipsoidal particles which are formed, displaced, and intruded into both fracture sides as the crack edges come in contact.

DOI: 10.1134/S1029959921010112

Keywords: very high cycle fatigue, aluminum alloy, fractography, fracture mechanisms, spherical particles

1. INTRODUCTION

In the context of physical mesomechanics and synergetics [1, 2], any loaded metal is an open system evolving successively on the micro-, meso-, and macroscales [3]. The range of very high cycle fatigue in metals, which corresponds to the microscale, spans to more than 10^8 loading cycles and reflects their behavior under long-term operation [4]. Metals can show very high cycle fatigue behavior with transitions to low or high cycle fatigue depending on the ratio $\sigma_{-1}/\sigma_{0.2}$, where σ_{-1} is the fatigue limit of a metal and $\sigma_{0.2}$ is its yield strength (Fig. 1) [5].

The essential feature of very high cycle fatigue is subsurface crack nucleation [4–9]. Its thorough studies in high-strength steels [8] and titanium alloys [9] suggest that the start point of a subsurface crack can be an inclusion, an interface of structural elements, and a flat facet of fracture along a structural element and that all these fracture nuclei first get surrounded with a fine crystalline zone. Among the possible factors responsible for such a zone in a material are compressive stresses which arise in unloading half-cycles and bring the material into a plastic state with its transition to a nanostructural state [8].

Once the nucleus of a subsurface crack is surrounded with a fine crystalline zone, the crack starts growing with the formation of fracture elements similar to those left by through-thickness cracks at a threshold velocity of less than 10^{-8} m/cycle. As the crack reaches the surface, its velocity increases steeply and the material fails, which makes the stages of its evolution hidden.

The fracture of aluminum alloys in the mode of very high cycle fatigue is addressed in a few studies [4, 10–15] and primarily because their fatigue curves lack a clear-cut plateau in the range of 10^7–10^8 cycles.

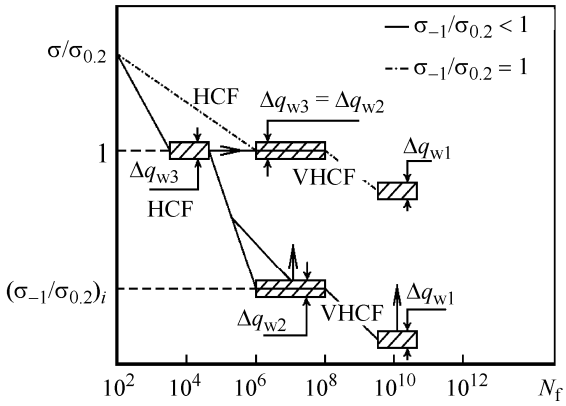

Fig. 1. Three-stage diagram of metal fatigue with bifurcation regions Δq_{wi} and bimodal life distribution on mesoscale [5]: HCF—high cycle fatigue, VHCF—very high cycle fatigue.

Table 1. Chemical composition of D16T aluminum alloy (wt %)

Fe	Si	Mn	Cr	Ti	Al	Cu	Mg	Zn	Ti+Zr	Impurity
<0.5	<0.5	0.3–0.9	<0.1	<0.15	90.9–94.7	3.8–4.9	1.2–1.8	<0.25	<0.2	<0.15

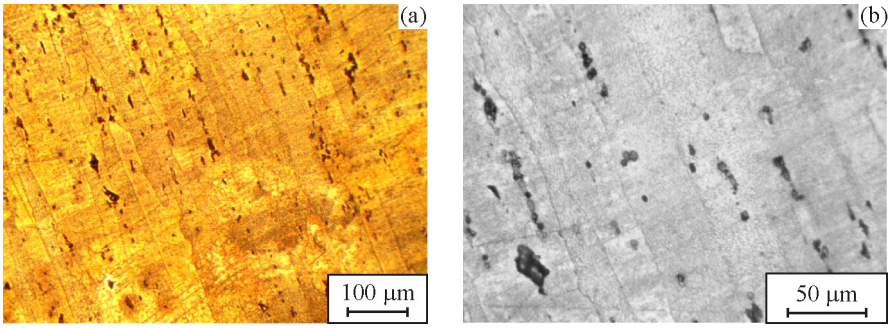

Fig. 2. Structure of D16T aluminum alloy at different magnifications (color online).

Hence, the idea of a fatigue limit introduced for high-strength materials is inapplicable to aluminum alloys.

Nevertheless, as has been shown [3, 4], aluminum alloys in very high cycle fatigue have a bimodal life distribution in the meso-to-micro transition region of damage accumulation such that two different fracture mechanisms are possible in two different specimens of the same material at a constant stress level. One specimen will get a crack nucleus on the surface and the other beneath the surface, and the probability of either of the two mechanisms will vary with stresses in the meso-to-micro transition region. Evidently, the probability of surface crack nucleation is higher at higher stresses, and that of subsurface crack nucleation is higher at lower stresses [3, 7].

Among the aluminum alloys is D16T alloy, which is a widely used aircraft material operating under high-frequency low-amplitude stress (fuselage and other frame elements, bulkheads, etc.). By now, the behavior of this material under very high cycle fatigue loads (more than 10^8 cycles) is uncertain and so are its safety margin and ultimate service life.

Presented below are the results of research on the behavior of D16T aluminum alloy in very high cycle fatigue at a cycling frequency of about 20 kHz.

2. RESEARCH TECHNIQUE

The test material was D16T aluminum alloy whose chemical composition is tabulated in Table 1. The material was supplied as hot-rolled bars of diameter 12 mm with a texture oriented along the bar axis (Fig. 2). Its tensile specimens were shaped so that the bar axis and the tension direction coincided. Thus, the mechanical characteristics of the material in tension were assessed crosswise the texture orientation. Their values under standard test conditions are presented in Table 2.

The specimen geometry for very high cycle fatigue fit the principles of high-frequency fatigue testing [4]: a dumbbell-shaped cylinder with a face section diameter of 10 mm and minimum gage section diameter of 3 mm on a radius of 31 mm (Fig. 3a).

The resonant length of a test specimen depends on its geometry (maximum and minimum cross sections), elastic characteristics (dynamic modulus E_d), density, and working frequency. For D16T aluminum alloy, the resonant length at a frequency of 20 kHz is L = 16.5 mm. As it follows from a harmonic finite element analysis (Fig. 3b), the normal stress in the specimen gage section is 9.5 MPa for resonant displacements of 1 μm at one of the specimen ends.

In the elastic range, the stress–displacement problem is linear, allowing stress estimations at larger displacements. In our experiments, we used a testing machine providing a displacement level of 5 to 40 μm.

The testing machine for very high cycle fatigue (VHCF) comprises the following control and executive devices: a personal computer with appropriate software, a high-precision data exchange card, a BRANSON DCX222 high-frequency generator for PC signal conversion to high-frequency electric oscillations with specified parameters, and a BRANSON 20RC piezoelectric converter for their conversion to vibrations of the same frequency. The converter with its piezoelectric crystals provides free vibrations in the

Table 2. Mechanical characteristics of D16T aluminum alloy

Parameter	E, GPa	σ_B, MPa	$\sigma_{0.2}$, MPa	δ, %	HV
Value	74	390	260	9	130

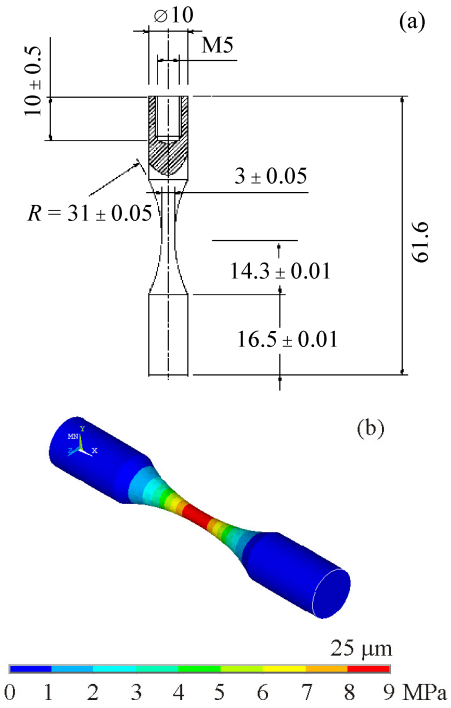

Fig. 3. Specimen geometry (mm) for high-frequency testing (a) and stresses at 1-μm displacements (b) according to finite element simulation (color online).

range from 19.5 to 20.5 kHz, and its highly efficient feedback allows efficient displacement control. For increasing the amplitude of mechanical vibrations, a booster (waveguide) is connected to the converter. The booster, like all other elements, fits the general principles of high-frequency loading.

The booster geometry provides the generation of a standing longitudinal elastic compression–extension wave with a frequency of 20 kHz. The eigenfrequencies of the booster and converter are the same. All other mechanical elements (horn, specimen) are similar in design to the booster, allowing a loading frequency of 19.5–20.5 kHz. The connection of all these elements is with inner steel screws.

Figure 4 shows the stress distribution in the machine at a frequency of 20 kHz for displacements of 1 μm applied to the booster base; the displacement at the specimen face, in this case, is larger than 1 μm. As can be seen, the maximum stress falls on the specimen gage section. All parasitic vibrations (bending, torsion) are outside the operating range of the converter. Numerical simulation data show that when exposed to progressive fracture on the VHCF machine, the majority of aluminum alloys, including D16T, continue to be loaded by the machine even if their specimens are broken into halves, and the cause of this is an insufficient frequency drop. According to our numerical simulation,

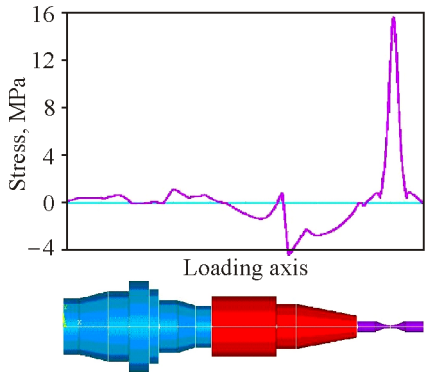

Fig. 4. Stress distribution in testing machine and in test Al specimen (color online).

the eigenfrequency of the machine operating with D16T aluminum alloy decreases by no more than 200 Hz when half of its specimen is split off. The simulation also shows that the free surface at the instant of failure does not experience any tensile stress, and hence, the fracture surface degrades little after separation of two specimen parts.

The temperature of the specimen surface throughout the test was kept constant via dry air cooling at 5°C. The maximum number of cycles to failure was $N_f = 10^{10}$.

3. RESEARCH RESULTS

Our tests suggest that in the specified stress range leading to $N_f = 2.8 \times 10^8$–5.1×10^9 cycles, the material fails in the transition region from very high to high cycle fatigue (Fig. 5) and that its fatigue strength decreases drastically as N_f is increased. Any asymptotic behavior of the material escapes detection.

Decreasing the load amplitude decreases the experimental data scatter because most of the fracture falls on the mode of very high cycle fatigue. In our experiments, the stress amplitude σ_a (MPa) and the

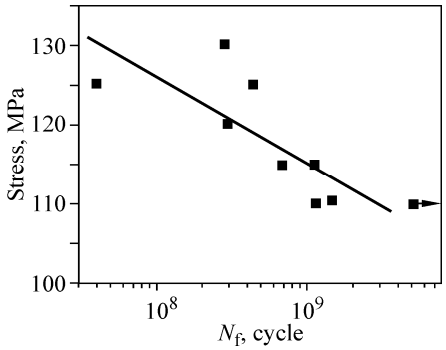

Fig. 5. Fatigue curve of D16T aluminum alloy in transition region from very high to high cycle fatigue at 20 kHz.

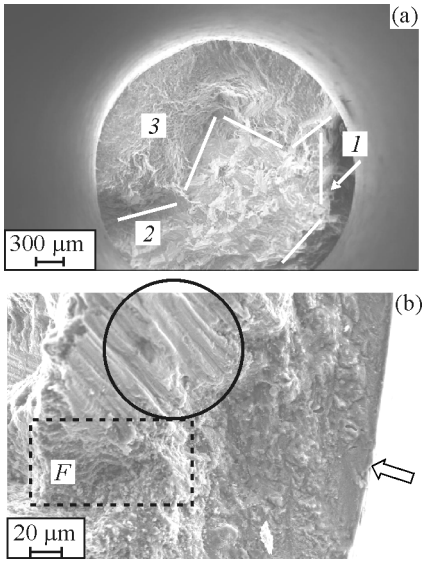

Fig. 6. Specimen fracture differing in morphology after 5×10^8 cycles (a) and fatigue crack growth from surface (b) with arrow for surface, circle for its damaged part, and square for transition to zone *2* with spherical fretting particles (zone *F*).

number of cycles to failure N_f are related as

$$\sigma_a + 4.75 \ln N_f = 213.6. \quad (1)$$

From fractographic data it follows that the test specimens are fractured both from their surface (downward) and from beneath it (upward) by the same three-stage mechanism.

Figure 6 exemplifies the three-stage fracture from the surface. First, a crack develops to a small depth, products at an angle of about 90° to the specimen axis (zone *1*). Next comes a cascade of quasi-brittle facets forming a fracture surface with clear black fretting oriented, on average, at 45° to the specimen axis (zone *2*). Finally, a rupture appears and the specimens fails (zone *3*).

In all fractures between zones *1* and *2*, there is a transition region covered with black fretting products (zone *F*) which represent a metal oxide layer with a cascade of spherical particles. The formation of such particles during the growth of fatigue cracks in aluminum alloys is described elsewhere [16].

In some specimens, the nucleation of a surface crack showed no sign of clear-cut fretting products (Fig. 7). The surface relief had the form of streaks pointing to transgranular fracture and allowing one to reliably judge the fracture focus position and the fatigue crack direction. However, between the initial and the next zone of fracture, there did exist a transition region with fretting products as a cascade of differently shaped particles and as evidence for contact interaction of the crack edges. In other specimens, the initial fracture zone developed from a focus located somewhat beneath their surface. In one case, two subsurface foci were detected in the material (Fig. 8): a fracture focus in the form of a flat facet bounded by an ellipse directly at the surface and a focus at some

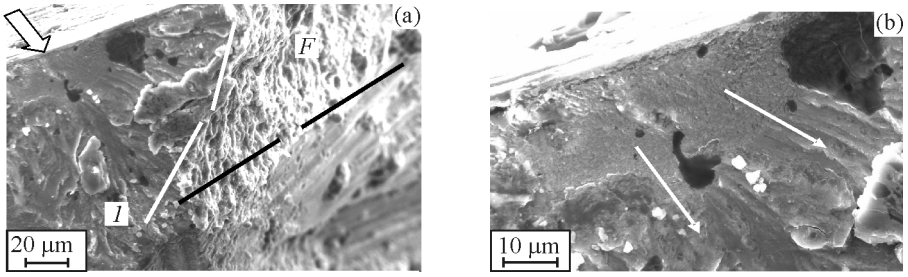

Fig. 7. Fracture nucleus after 10^6 cycles with indication of crack growth direction (white arrows) and transition from fracture zone *1* to zone *2* with fretting products.

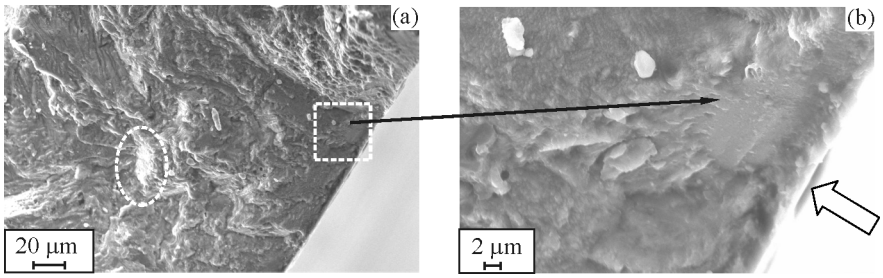

Fig. 8. Fracture zone *1* after 5×10^7 cycles with indication of surface (arrow), surface nucleus (square), and subsurface nucleus (circle).

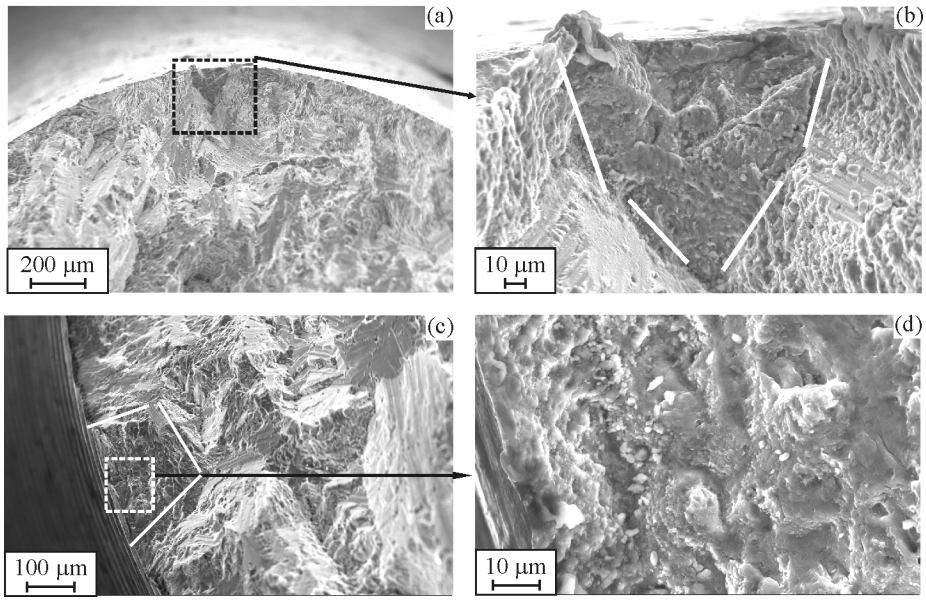

Fig. 9. Fracture zone *1* with fretting products for subsurface crack nucleation at grain boundary after 10^7 (a, b) and 10^8 cycles (c, d).

distance from it. The initial fracture zone contained streaks with spherical fretting particles suggesting that its sides came in contact during crack propagation.

In another case, a fracture focus at grain boundaries was formed somewhat beneath the surface (Figs. 9a, 9b). The density of fretting products varied depending on the conditions of crack nucleation and growth from grain boundaries. This is because the plastic strain in the material is constrained during subsurface crack propagation.

In view of the foregoing, it is of interest to analyze the fracture of that specimen which first did not fail after 1.45×10^9 cycles at 110 MPa and then did fail after 15.4×10^7 cycles at 130 MPa. Our analysis shows that the crack in the specimen nucleated at grain boundaries beneath the surface (Fig. 10). Its initial fracture zone *1* was almost perpendicular to the specimen axis and was shaped as a clear-cut ellipse with a streak relief. At the boundaries of the zone, fretting products were formed as a cascade of spherical and semiellipsoidal particles. From this it follows that the specimen could be prepared for the formation of zone *1* at the stage of its initial loading at 110 MPa. Under further loading at 130 MPa, its crack grew through weakened points of zone *1* with some delay of fracture due to a large amount of fretting products appearing along the boundaries of zone *2*. As the crack edges came in contact, the crack growth was arrested.

The crack growth through zone *2* was the same in all specimens, featuring narrow extended facets of quasi-brittle fracture (Fig. 11). Such a relief is atypical for aluminum alloys operating at low temperature and featuring a dimple relief characteristic of ductile fracture. Here, quasi-brittle means that the material experienced ductile fracture but with pronounced slip along the weakest planes and did not experience any embrittlement. The conclusion is evident from the test procedure: the specimen temperature under high-fre-

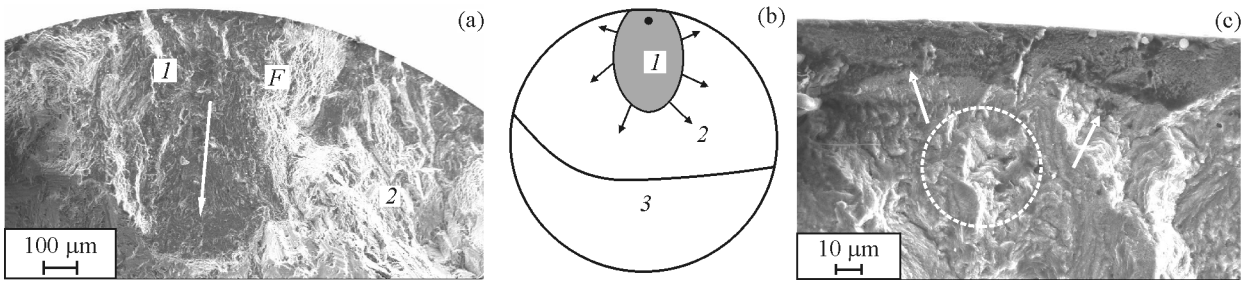

Fig. 10. Fracture zones *1*, *2* and transition *F* covered with fretting products (a), their diagram with fracture focus marked by black solid circle (b), and near-focus transgranular fracture marked by dashed circle with arrows for crack direction (c).

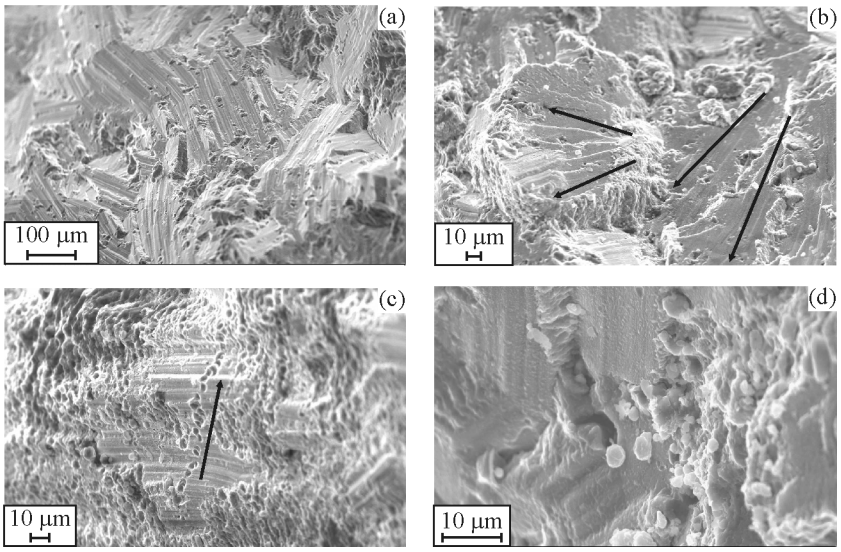

Fig. 11. Fracture relief in zone *2* after 5×10^8 (a), 10^7 (b), 10^8 (c), and 10^9 cycles (d) with arrows for crack direction (b) and direction of spherical particles leaving cascade of dimples (c).

quency loads can only increase but, as has been shown, to no more than 150°C even in subsurface crack nuclei [4]. This fact is also confirmed by the presence of spherical and ellipsoidal fretting particles in zone *2*. Earlier, such particles in aluminum alloys were referred to artifacts [13, 15]. When the edges of a propagating crack are slightly open, these particles can migrate due to rotations of material volumes: they can intrude into one fracture side and then into the other as the two sides are displaced and come in contact (Fig. 12). As a result, a cascade of oriented dimples replicating the geometry of intruded particles are

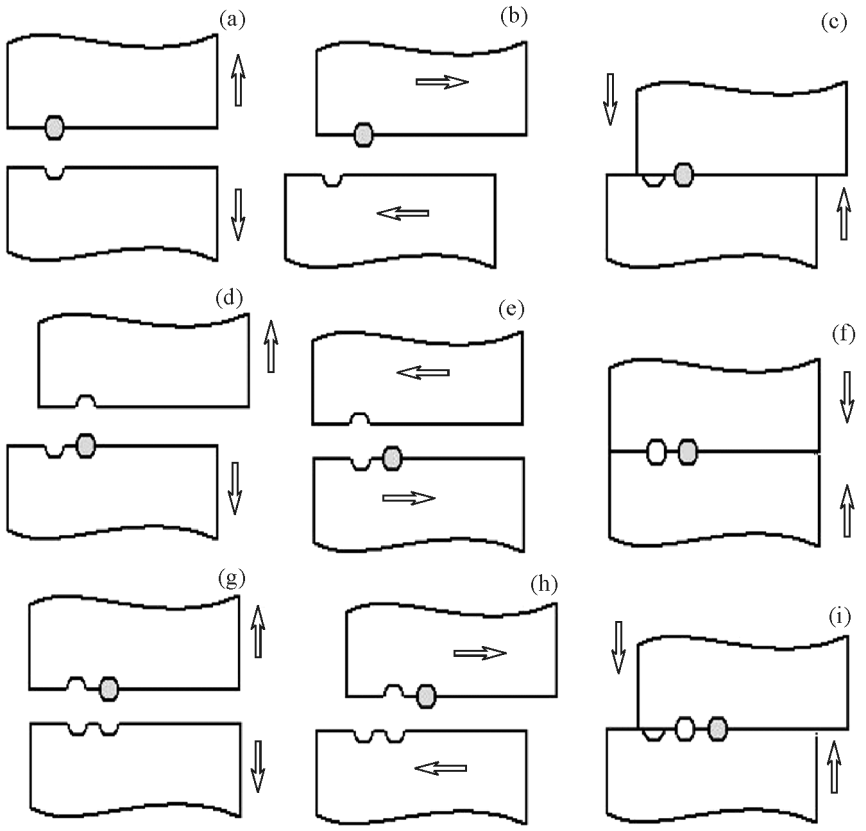

Fig. 12. Diagram of successive intrusion of spherical particles into both fracture sides via shear and crack opening.

left on the fracture surface (Fig. 11c) while the particles as such can be found in zones spaced from their parent dimples (Fig. 11d). Thus, the particles can migrate between the crack edges without any substantial damage to the fracture surface because no direct contact is available for reciprocally oriented facets in zone *2*.

Some zones reveal fretting products at the boundaries of steps formed by fracture along a cascade of slip planes (Fig. 13). These fretting products represent ellipsoidal particles whose axes are oriented almost perpendicular to slip planes passed through fracture. The ellipsoidal form of particles confirms the fact of quasi-brittle fracture by shear along slip planes. In zone *3*, all specimens were identical in their dimple fracture relief as typical of D16T aluminum alloy at the instant of failure.

4. ANALYSIS OF RESEARCH RESULTS

Our study suggests that D16T aluminum alloy at its transition from high to very high cycle fatigue can be fractured from the surface and from beneath the surface at the same stress level, which has also been found in hardened and unhardened 2024T3 aluminum alloy at different loading frequencies [4, 11].

The behavior of fretting products is governed mainly by the behavior of a crack as it propagates with contact interaction of its edges along a crooked path in the space of incipient quasi-brittle fracture facets. The formation of differently shaped fine particles suggests that the crack edges are displaced slightly and that the fracture is dominated by mode II along incipient unit facets. Such a pattern of fracture differs radically from what is observed in aluminum alloys under cyclic loads, and its features are associated more with high load frequencies than with low load amplitudes. In this case, the metal has no time to relax the energy supplied in each cycle such that the most beneficial way of energy dissipation in the metal is by shear in differently oriented planes.

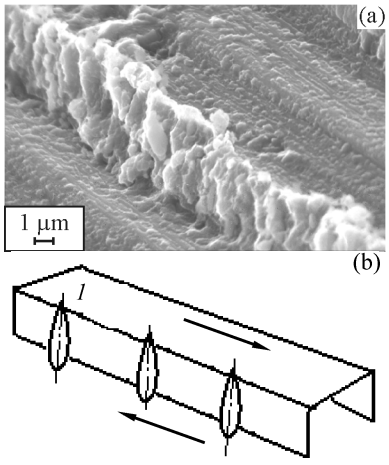

Fig. 13. Transition from flat surface *1* in zone *2* to surface with cascade of ellipsoidal fretting particles (a) and diagram of their formation during crack growth (b).

It is significant that the test alloy can start fracturing from flat quasi-brittle facets with the formation of a streak fracture relief (Fig. 7). Such a relief is typical for the first stage of metal fracture at a crack velocity of less than 10^{-8} m/cycle and is conventionally associated with mode II [7]. This comes in contrast with the next fracture stage which reveals only quasi-brittle facets and in which the crack velocity should be higher but the elements of the relief point to pronounced shear fracture.

However, the fracture relief formed at low crack velocities under low-frequency loads is radically different from that found in zone *2* in our study. From this it follows that mode II fracture as dominant early in the crack growth with low velocities at low frequencies does not correspond to pure shear. Moreover, the streak relief observed in zone *1* in our study is analogous to that under low-frequency loads.

The fracture pattern in zone *2* with its cascade of quasi-brittle facets suggests that at high load frequencies the material shows less plasticity than it does during slow crack propagation at low frequencies. Typically, fatigue striations appear in aluminum alloys as their cracks get faster, and in our case, there appears a cascade of quasi-brittle facets.

The above fact should be considered significant for proper fracture diagnostics: in D16T aluminum alloy, the presence of quasi-brittle facets points to its high-frequency loading.

5. CONCLUSION

Our study of D16T aluminum alloy shows that its behavior at the transition from very high to high cycle fatigue follows a three-stage fracture mechanism.

First, a crack nucleus appears either on the surface at a quasi-cleavage facet or beneath the surface at a grain boundary with crack propagation almost perpendicular to the specimen axis. Next, the fracture changes the macroscopic orientation such that its angle about the specimen axis becomes equal, on average, to 45°. Finally, the fracture forms a dimple relief and switches to failure. All these three stages have a clear-cut boundary in between.

At the first stage of crack growth, a layer of fretting products appears in fracture zone *1*, and then,

spherical fretting particles at its transition to zone *2*. Such spherical particles are also found in zone *2* against the formation of quasi-brittle fracture facets.

The second stage of crack growth is governed by shear which results in quasi-brittle fracture facets oriented at different angles to the specimen axis. Such a relief differs radically from what is observed in D16T aluminum alloy under high cycle fatigue loads.

The formation and the behavior of spherical and ellipsoidal particles are conditioned by rotations of material volumes, allowing their migration from one fracture side to the other as the crack edges come in contact. Our data suggest that such contact interaction occurs at both stages of crack growth (zones *1*, *2*) but the interaction conditions differ due to different stress states in the material. At the final stage, the material fails with the formation of a dimple relief.

FUNDING

The work was supported by the Russian Science Foundation (project No. 19-19-00705).

REFERENCES

1. Panin, V.E., Synergetic Principles of Physical Mesomechanics, *Phys. Mesomech.*, 2000, vol. 3, no. 6, pp. 5–34.
2. Ivanova, V.A., *Synergetics*. *Strength and Fracture of Metal Materials*, Moscow: Nauka, 1992.
3. Shanyavsky, A.A., Scales of Metal Fatigue Cracking, *Phys. Mesomech*., 2015, vol. 18, no. 2, pp. 163–173. doi 10.24411/1683-805X-2014-00067
4. Bathias, C. and Paris, P.C., *Gigacycle Fatigue in Mechanical Practice*, New York: Marcel Dekker, 2005.
5. Shanyavskiy, A.A. and Soldatenkov, A.P., Scales of Metal Fatigue Limit, *Phys. Mesomech*., 2020, vol. 23, no. 2, pp. 120–127. doi 10.1134/S1029959920020034
6. Murakami, Y., *Metal Fatigue: Effects of Small Defects and Non-Metallic Inclusions*, Elsevier Science Ltd., 2002.
7. Shanyavsky, A.A., *Simulation of Fatigue Fracture of Metals*. *Synergetics in Aviation*, Ufa: Monografiya, 2007.
8. Shanyavskiy, A.A., Self-Organization of Nanostructures in Metals under Ultrahigh Cycle Fatigue, *Fiz. Mezomekh*., 2012, vol. 15, no. 5, pp. 91–105.
9. Shanyavskiy, A., Scale of Metal Fatigue Failures and Mechanisms for Origin of Subsurface Fracture Formation, *Solid State Phenomena*, 2017, vol. 258, pp. 249–254.
10. Carboni, M., Annoni, M., and Ferraris, M., Analyses of Premature Failure of Some Aluminum Alloy Sonotrodes for Ultrasonic Welding, *Proc. V Int. Conf. Very High Cycle Fatigue, VHCF5, DVM, June 28–30, 2011*, Berger, C. and Christ., H.-J., Eds., Berlin, 2011, pp. 589–594.
11. Shanyavskiy, A., Mechanisms of the 2024-T351 Al-Alloy Fatigue Cracking in Bifurcation Area after Laser Shocks Hardening Procedure, *Key Eng. Mater.*, 2011, vol. 465, pp. 511–514.
12. Schwerdt, D., Pyttel, B., and Berger, C., Microstructure Investigations with SEM, EBSD and TEM on Cyclic Stressed and Unstressed Specimens of Two Different Aluminium Wrought Alloys, in *Proc. V Int. Conf. Very High Cycle Fatigue, VHCF5, DVM, June 28–30, 2011*, Berger, C. and Christ., H.-J., Eds., Berlin, 2011, pp. 207–212.
13. Banhart, J., Chang, C.S.T., Liang, Z., Wanderka, N., Lay, M.D.H., and Hill, A.J., Natural Aging in Al–Mg–Si Alloys—A Process of Unexpected Complexity, *Adv. Eng. Mater.*, 2010, vol. 12, no. 7, pp. 559–571.
14. Mayer, H., Fitzka, M., and Schuller, R., Ultrasonic Fatigue Testing of 2024-T351 Aluminium Alloy at Different Load Ratios under Constant and Variable Amplitude, in *Proc. V Int. Conf. Very High Cycle Fatigue, VHCF5, DVM, June 28–30, 2011*, Berger, C. and Christ., H.-J., Eds., Berlin, 2011, pp. 355–360.
15. Kawagoishi, N., Kariya, K., Wang, Q.Y., Maeda, Y., and Goto, M., Effect of Loading Frequency on Fatigue Crack Growth of Age-Hardened Al Alloy, in *Proc. V Int. Conf. Very High Cycle Fatigue, VHCF5, DVM, June 28–30, 2011*, Berger, C. and Christ., H.-J., Eds., Berlin, 2011, pp. 269–274.
16. Shaniavski, A.A., Rotational Instability of Mesoscale Deformation and Fracture of Metals in Fatigue Crack Propagation. I. Plastic Deformation at the Crack Tip, *Phys. Mesomech.*, 2001, vol. 4, no. 1, p. 67–74.